Optics Letters

3D thickness map reconstruction of dielectric thin films using scattering of surface plasmon polaritons

Cesar E. Garcia-Ortiz,[1,*] Rodolfo Cortes,[1] Robin Orejel,[2] Raul Hernandez-Aranda,[2] Israel Martínez-López,[2] Félix Aguilar,[3] and Victor Coello[1]

[1]CICESE, Unidad Monterrey, Alianza Centro 504, PIIT Apodaca, NL 66629, Mexico
[2]Tecnológico de Monterrey, Eugenio Garza Sada 2501 Sur, Monterrey, NL 64849, Mexico
[3]INAOE, Luis Enrique Erro No. 1, Sta. Ma. Tonantzintla, Puebla 72800, Mexico
*Corresponding author: cegarcia@cicese.mx

Received 12 December 2017; revised 5 January 2018; accepted 7 January 2018; posted 9 January 2018 (Doc. ID 315583); published 7 February 2018

Thin films are key elements in the current development of nanotechnology, and their characterization has become an essential task. In this Letter, we report on a technique to reconstruct full 3D maps of dielectric thin films using the scattered light of decoupled surface plasmon polaritons. Patterned magnesium fluoride thin films were fabricated, and their 3D thickness map was fully reconstructed with high (<1 nm) precision. This technique can be applied and easily adjusted to identify inhomogeneities in wide areas (mm^2 – cm^2) of dielectric samples with subnanometer precision, or to characterize the fabrication processes involved in the preparation of patterned multilayered systems. © 2018 Optical Society of America

OCIS codes: (240.6680) Surface plasmons; (310.6860) Thin films, optical properties; (310.6870) Thin films, other properties; (310.4165) Multilayer design; (100.0100) Image processing; (120.5820) Scattering measurements.

https://doi.org/10.1364/OL.43.000691

The latest developments in various fields of modern nanotechnology require the use of thin-film coatings (<100 nm), such as in solar cells [1], optical sensors [2], photonic crystals [3], and plasmonic devices [4], among others. In most cases, the thickness of the films is a critical parameter and precision at the nanoscale is often required. Slight differences between the design and fabrication parameters can lead to significant variations from the expected results; thus, a precise characterization of the nanometer-sized films after fabrication is an important task. Thickness characterization techniques, such as spin-coating, thermal evaporation, sputtering, and molecular beam epitaxy [5], are also important to determine the quality of the fabrication methods used to produce the thin films.

There are several techniques to measure accurately the thickness of a thin-film coating, such as interferometry [6], ellipsometry [7], profilometry [8], and atomic force microscopy [9], to name a few. Moreover, spectrophotometry imaging, which is not a method based on surface plasmon resonance (SPR), has also been used to reconstruct the thickness of nonuniform non-absorbing thin films in millimeter-sized areas [10]. The phenomenon of SPR can also be exploited to determine the thickness of a thin film, if at least one of the films can support the generation of surface plasmon polaritons (SPPs) [11–15]. SPPs are evanescent electromagnetic modes confined to the interface between a metal and a dielectric, which are associated to collective oscillations of the electrons on the surface of a metal [16–18].

The penetration of SPPs into the dielectric is known as the penetration depth, i.e., the distance at which the intensity has decayed as $1/e$, and is typically on the order of half the wavelength. Within this region, the SPR is very sensitive to changes in the effective refractive index, which can be characterized in order to determine the thickness of potential thin-film-based multilayered systems.

The most common experimental setup used to estimate the thickness of a thin-film using the SPR, consists of reflectivity measurements with a Kretschmann configuration [19,20]. While this technique has been reported in the past to estimate the thickness of single monolayers of a lipid film [21], and a full reconstruction of the thickness map was obtained, the technique was strongly limited by the short thickness dynamic range of <10 nm. Such a limitation is intrinsic to the technique and cannot be overcome using the same setup or method, since it is a consequence of the single angle reflectivity measurements. In this Letter, we present a method to obtain wide (~mm^2) three-dimensional (3D) thickness maps of dielectric thin films, with subnanometer precision, using the scattering produced by SPPs. This technique allows us to reconstruct 3D thickness maps of the areas of interest that can be escalated to several square centimeters and with a thickness dynamic range of up to 100 nm with subnanometer precision.

The experimental setup consists of a Kretschmann configuration in which an imaging system was installed on the same

rotation stage as the prism (N-BK7), allowing us to take images with a charge-coupled device (CCD) camera of the same area of interest as the prism was rotated (Fig. 1). The purpose of the imaging system was to take optical images of the surface of the sample at different angles of excitation, and to use each of the pixels of the CCD camera as individual power detectors to register the intensity of the scattered light [22]. For our purposes, we used two lenses with the same focal distance, but this can be exchanged depending on the specific applications, e.g., a microscope objective could also be installed to study smaller areas with a higher resolution. The light source consisted of an He–Ne laser with an emission at 632 nm, which was expanded to a full width at half-maximum of ∼1 cm.

The samples used in this Letter consisted of thin magnesium fluoride (MgF_2) coatings (<100 nm), deposited via thermal evaporation on top of a 45 nm thick gold film, used to couple SPPs, on a glass substrate. The samples were positioned at the hypotenuse of a right angle prism, using index-matching oil. In contrast to typical reflectivity measurements, we detected the scattered light produced by SPPs that are decoupled by the local roughness of the films. This phenomenon is caused by the strong field enhancement generated by the SPPs at the interface, and it can be used to estimate the thickness of the films and the optical parameters of the system, since the intensity of the scattered light is proportional to the amplitude of the evanescent field [16,23–25]. A set of four samples (A, B, C, and D) with different MgF_2 film thickness was fabricated, in order to validate the effectivity of the technique by comparing reflectivity versus scattering measurements [Fig. 2(a)]. The reflectivity was simply measured with a power meter, while the scattered light was detected with the CCD camera (Thorlabs DCU223M) by integrating the intensity values of all the pixels in the camera [Figs. 2(b) and 2(c)]. Both approaches show well-defined resonances that can be analyzed through numerical fitting to find the thickness of the dielectric films, since the angular position of the SPR shifts as a consequence of the changes of the effective refractive index of the mode. The analytical expressions of multilayered systems used here can be found in [26,27]. The effective refractive index n_{eff} of the plasmonic mode was calculated using a rigorous semi-analytical method that consists of solving the Helmholtz equation for plasmonic multilayered systems, by finding the appropriate values of the propagation constant $\beta = k_0 n_{\mathrm{eff}}$ that satisfy the boundary conditions [28], where k_0 is the free-space wavevector. The effective index and the SPR angle θ_{Kr} in the Kretschmann configuration are directly related and can be calculated using the expression $\theta_{Kr} = \sin^{-1}(n_{\mathrm{eff}}/n_p)$, where n_p is the refractive index of the substrate [17]. The calculations of the effective refractive index of the plasmonic mode and its derivative as a function of the film thickness show that the most sensitive thickness interval goes from 10 to 150 nm, for MgF_2 coatings (Fig. 3).

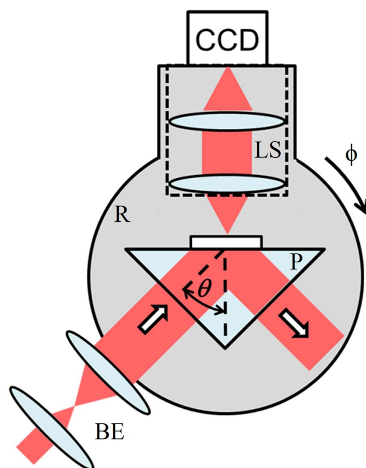

Fig. 1. Experimental setup which consists of a Kretschmann configuration where a CCD camera and a lens system (LS) have been attached to the same rotation stage (R) as the prism (P). The beam of the laser is expanded (∼1 cm) with a beam expander (BE) to illuminate the complete area of interest.

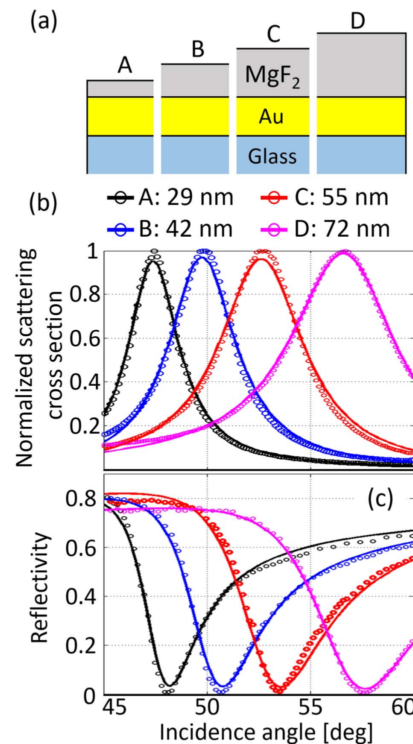

Fig. 2. (a) Schematic diagram of the geometrical parameters of the four fabricated samples with flat surfaces. (b) Scattering measurements (circles) obtained with the CCD camera and fit (solid lines). (c) Attenuated total internal reflection measurements (circles) detected with a power meter and fit (solid lines).

Nevertheless, for films thicker than 100 nm, the resonance angle surpasses 65°, which complicates the measurements for two main reasons: first, the spot of the laser starts to elongate and shift position faster, and cannot be considered as a constant intensity illumination at each point of the surface. Second, at large angles, the laser beam is partially blocked by the edges of the prism. It is worth mentioning that these parameters can be tailored depending on the specific application, for example, by changing the wavelength of the illumination source or the refraction index of the prism coupler.

The main motivation for this Letter was to obtain precise values of the thickness of a dielectric thin film at each point of the surface, e.g., to characterize the inhomogeneity of a thin film, in contrast to other methods which only give an average

value of a determined region [29,30]. For this purpose, we fabricated another set of samples on which a second layer of MgF_2 (20 nm) was deposited on top of a similar 20 nm thick MgF_2 film, where a vinyl mask was used to partially block the sample during the deposition process and create lithographic patterns to be reconstructed [Figs. 5(a) and 5(d)]. For our purposes, we used a mask with the image of a pelican (CICESE logo).

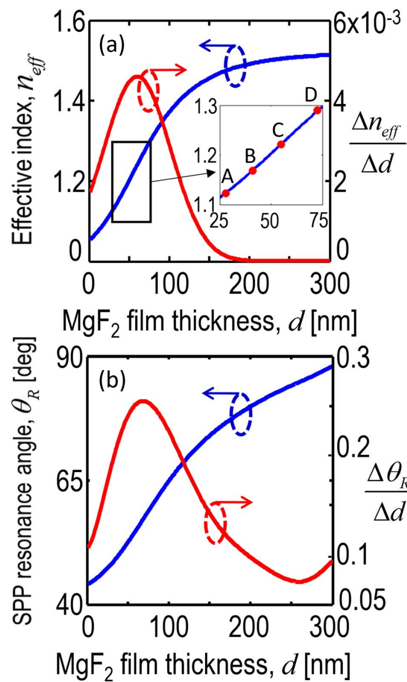

Fig. 3. (a) Effective refractive and its derivative as a function of the MgF_2 film thickness. The inset is a zoom of the region inside the black rectangle to show the effective index for the samples A–D. (b) SPP resonance angle and its derivative as a function of the MgF_2 film thickness.

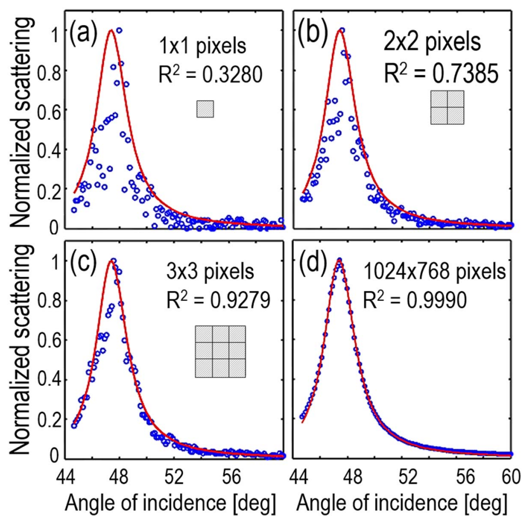

Fig. 4. Intensity measurements obtained from pixels in the CCD camera for averaged arrays of (a) 1×1, (b) 2×2, (c) 3×3, and (d) 1024×768 pixels. The red solid curve corresponds to the best numerical fit, and the correlation coefficient R^2 is labeled in each case.

The process to reconstruct 3D maps of the film thickness consists of two main steps. The first step is the same as described above for flat surfaces, i.e., images from the surface are taken at each angle and stored in a computer for further processing. An angular resolution of 0.1° was used in our measurements. The second step consists of an automated post-processing algorithm that runs a MATLAB script which finds the thickness of the film at each point of the surface, corresponding to every pixel of the camera, using a semi-analytical numerical fit (same mentioned for flat surfaces). Each pixel of the CCD camera was intended to act as individual power detectors in order to determine the intensity at every excitation angle; nevertheless, the signal-to-noise ratio turned out to be low if a single pixel was considered. We used the correlation coefficient R^2 of the fitting results as a figure of merit to determine the minimum amount of square pixels that would be necessary to average, in order to get a reliable experimental curve ($R^2 > 0.9$). The experimental data were fitted for arrays of 1×1, 2×2, and 3×3 pixels (Fig. 4). A value of $R^2 = 0.9279$ was found for the 3×3 array case, and this matrix is now considered a single pixel in the automated post-processing script. Even though the amount of pixels decreased from 1024×768 to 341×256, it is important to note the elevated number of fitting processes (87,296) required to obtain the final result, an unpractical, highly time-consuming task to be done by hand due to the elevated number of pixels.

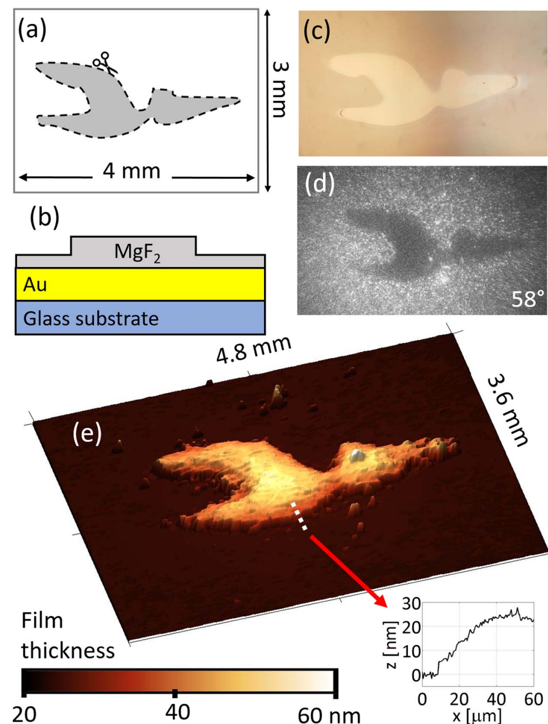

Fig. 5. (a) Diagram showing the design for the mask used to fabricate the sample. (b) Schematic diagram of the patterned multilayered system. (c) Optical microscope image in a reflection of the area of interest. (d) Scattered light at the SPP resonance angle (of the lower level) taken with the CCD camera. (e) Reconstructed 3D map of the MgF_2 film thickness. The inset corresponds to an atomic force microscope topography measurement of a transverse section x along the edge of the structure (dotted line).

Yet, using a single eight-core computer (3.60 GHz), working in parallel, took only 15 min to finish the process. Using this procedure, it was possible to obtain a full 3D reconstruction of the dielectric film thickness (Fig. 5). The details of the logo are clearly visible due to the high fidelity of the reconstructed image, as well as the height gradient which gives information about the deposition and mask removal processes. The standard deviation of the thickness was calculated in the flat regions surrounding the protuberance to estimate the precision of the measurements. The obtained results presented values below 1 nm, which are associated to the subnanometer precision of this technique. The areas of interest investigated in this Letter consisted of areas of tens of square millimeters, but the setup can be easily adjusted to reconstruct areas of square centimeters, simply by using a wider CCD camera, or changing the lens system (LS) to reduce the size of the image (Fig. 1).

In summary, we have presented a technique to reconstruct 3D thickness maps of dielectric thin films through the detection of scattered light from decoupled SPPs. The high sensitivity of the effective refractive index of SPPs to changes in the geometrical parameters of the multilayered systems allows very precise (subnanometer) determination of the local (point-by-point) thicknesses. It was possible to determine the thickness of the film for every pixel of the camera, associated to each point in the surface of the sample, using an automated post-processing algorithm based on numerical fitting. This technique can be applied to investigate macroscopic inhomogeneities in dielectric thin films, as well as wide-area designed patterns in arrays of multilayered systems with high fidelity and precision. The wide field of view (mm^2 – cm^2) available with this technique, dynamic range, and high precision (subnanometer) makes it an engaging alternative for wide-area characterization of dielectric thin films. Different deposition methods and equipment can also be studied, characterized, and compared in more detail using the capabilities of this technique.

Funding. Consejo Nacional de Ciencia y Tecnología (CONACYT) (250719, 252621).

REFERENCES

1. P. M. Kaminski, F. Lisco, and J. M. Walls, IEEE J. Photovoltaics **4**, 452 (2014).
2. M. Yang and J. Dai, Photon. Sens. **2**, 14 (2012).
3. F. Villa, J. A. Gaspar-Armenta, and F. Ramos-Mendieta, Opt. Commun. **216**, 361 (2003).
4. C. García, V. Coello, Z. Han, I. P. Radko, and S. I. Bozhevolnyi, Opt. Express **20**, 7771 (2012).
5. A. Piegari and F. Flory, *Optical Thin Films and Coatings: From Materials to Applications*, 1st ed. (Woodhead, 2013).
6. S. Mamedov, A. D. Schwab, and A. Dhinojwala, Rev. Sci. Instrum. **73**, 2321 (2002).
7. D. Lehmann, F. Seidel, and D. R. Zahn, SpringerPlus **3**, 82 (2014).
8. A. Piegari and E. Masetti, Thin Solid Films **124**, 249 (1985).
9. R. F. M. Lobo, M. A. Pereira-da-Silva, M. Raposo, R. M. Faria, and O. N. Oliveira, Jr., Nanotechnology **10**, 389 (1999).
10. M. Ohlídal, V. Cudek, I. Ohlídal, and P. Klapetek, Proc. SPIE **5963**, 596329 (2005).
11. W. P. Chen and J. M. Chen, J. Opt. Soc. Am. **71**, 189 (1981).
12. H. E. de Bruijn, B. S. F. Altenburg, R. P. H. Kooyman, and J. Greve, Opt. Commun. **82**, 425 (1991).
13. J. H. Gu, Z. Q. Cao, Q. S. Shen, and G. Chen, J. Phys. D **41**, 155309 (2008).
14. L. Lévesque, Opt. Laser Technol. **43**, 14 (2011).
15. C. Liu, Q. Liu, Z. Qin, and X. Xie, Plasmonics **12**, 1199 (2016).
16. H. Raether, *Surface Plasmons on Smooth and Rough Surfaces and on Gratings*, 1st ed. (Springer, 1988).
17. S. A. Maier, *Plasmonics: Fundamentals and Applications*, 1st ed. (Springer, 2007).
18. J. Zhang, L. Zhang, and W. Xu, J. Phys. D **45**, 113001 (2012).
19. E. Fontana, Appl. Opt. **45**, 7632 (2006).
20. C. Liu, Q. Liu, and X. Hu, Opt. Express **22**, 7574 (2014).
21. H. Morgan and D. M. Taylor, Appl. Phys. Lett. **64**, 1330 (1994).
22. H. P. Ho and W. W. Lamb, Sens. Actuators B **96**, 554 (2003).
23. A. Giannattasio, I. R. Hoope, and W. L. Barnes, Opt. Express **12**, 5881 (2004).
24. B. H. Ong, X. Yuan, S. C. Tjin, J. Zhang, and H. M. Ng, Sens. Actuators B **114**, 1028 (2006).
25. A. Ono, M. Kikawada, R. Akimoto, W. Inami, and Y. Kawata, Opt. Express **21**, 17447 (2013).
26. C. C. Katsidis and D. I. Siapkas, Appl. Opt. **41**, 3978 (2002).
27. H. R. Gwon and S. H. Lee, Mater. Trans. **51**, 1150 (2010).
28. H. T. Baltar, K. Drozdowicz-Tomsia, and E. M. Goldys, *Plasmonics—Principles and Applications* (InTech, 2012), Chap. 6.
29. H. E. de Bruijn, M. Minor, R. P. H. Kooyman, and J. Greve, Opt. Commun. **95**, 183 (1993).
30. T. Del Rosso, J. E. Hernández Sánchez, R. D. Santos Carvalho, O. Pandoli, and M. Cremona, Opt. Express **22**, 18914 (2014).

158.97.112.15 {ts '2018-02-06 12:42:05'}